Investigation of prompt fission neutron (PFN) emission in $^{235}U(n_{th}, f)$ *reaction*

Zeynalov Sh. Sedyshev P., Sidorova O.,Shvetsov V.

JINR-Joint Institute for Nuclear Research, Dubna, Russia

1. Motivation

The mechanism of PFN emission in fission plays important role in nuclear fission theory from the one hand and the information on PFN is highly demanded by nuclear power industry from the other hand.

Analysis of TKE measured in resonance neutron induced fission of ^{235}U revealed surprising fluctuation. The recent measurement of PFN multiplicity in ^{235}U resonances demonstrates fluctuations of PFN multiplicities to.

One of the interesting observation is the increasing $\bar{\nu}(A)$ from the heavy FF with increase of the excitation energy of fissioning system still has no clear explanation

In current report we presenting some preliminary results of measurement of PFN emission in thermal neutron induced fission of ^{235}U as test of apparatus for resonance neutron induced fission of ^{235}U measurements foreseen to perform at IREN facility next year

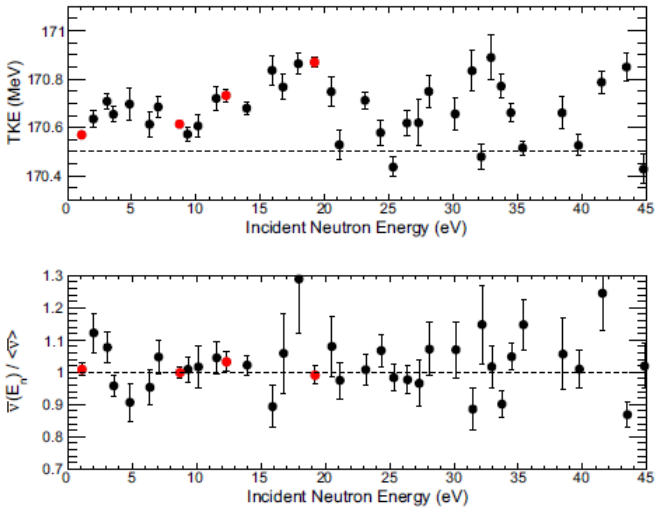

EPJ Web of Conferences **111**, 05001 (2016)
DOI: 10.1051/epjconf/201611105001

2. Experimental setup and data acquisition system.

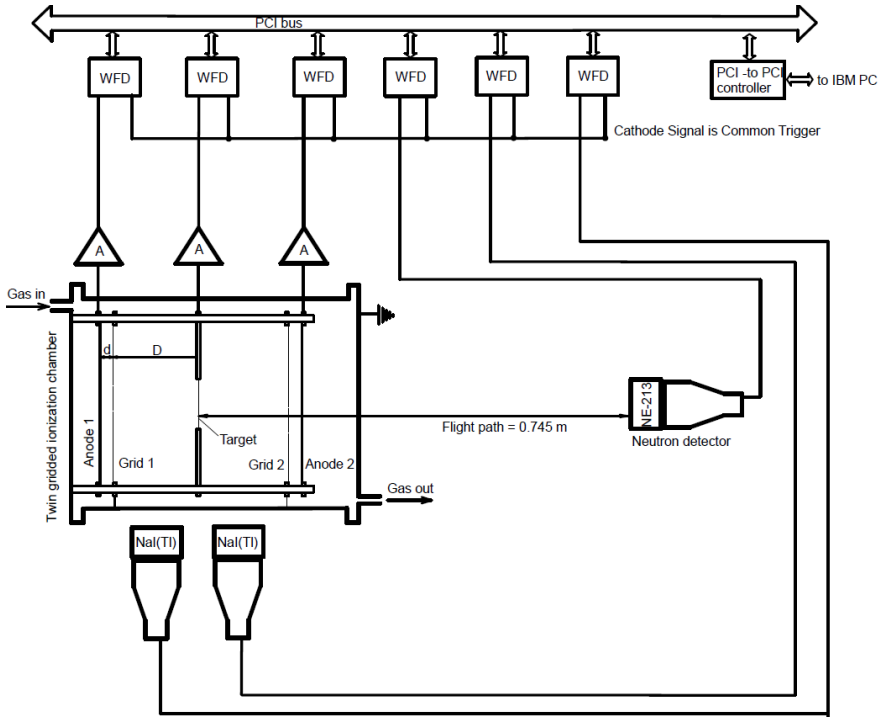

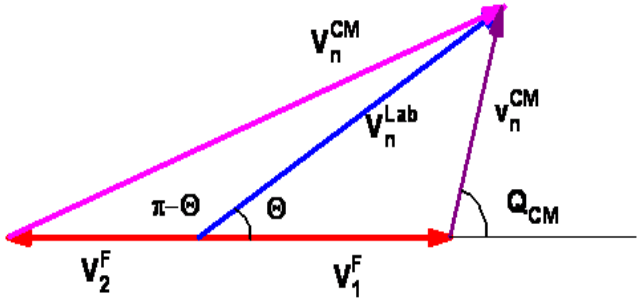

$$\bar{\nu}(A)=\frac{\int_0^{\infty}\nu(A,TKE)Y(A,TKE)dTKE}{\int_0^{\infty}Y(A,TKE)dTKE},\quad \bar{\nu}=\int_0^{\infty}\nu(A,TKE)Y(A,TKE)dTKEdA,\quad 200=\int_0^{\infty}Y(A,TKE)dTKEdA$$

$$\bar{\nu}(TKE)=\frac{\int_0^{\infty}\nu(A,TKE)Y(A,TKE)dA}{\int_0^{\infty}Y(A,TKE)dA},\quad \bar{\nu}=\int_0^{\infty}\nu(A,TKE)Y(A,TKE)dTKEdA,\quad 200=\int_0^{\infty}Y(A,TKE)dTKEdA$$

Adopted from C. Budtz-Jørgensen and H.-H. Knitter, *Nucl. Phys.*, A490, 307(1988) and modified with digital pulse processing apparatus

3. Digital Pulse Processing (DPP).

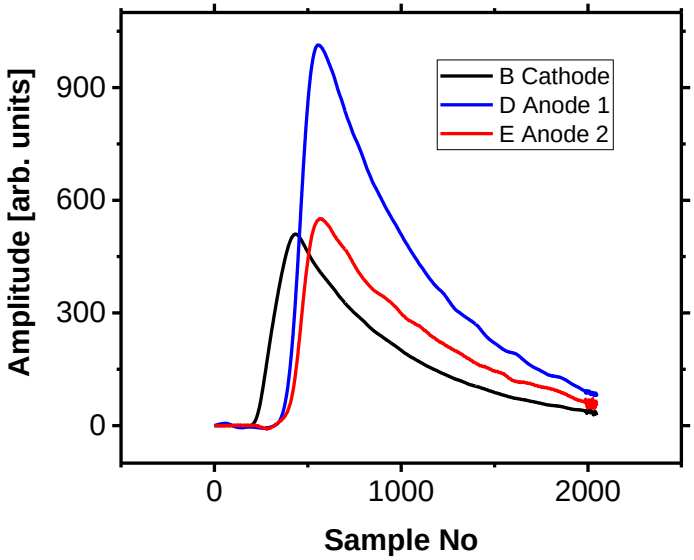

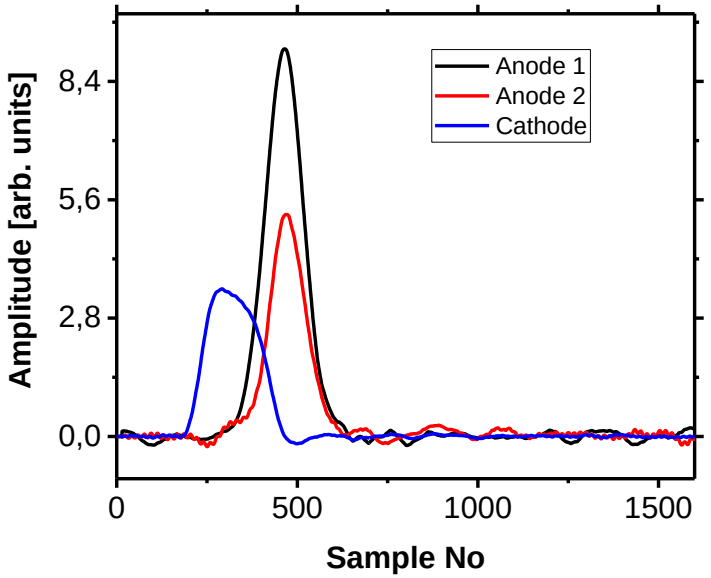

In our approach we have oversampled FF signals. The oversampling we used to increase the effective number of bits (ENOB) improving the signal representation. In practice the increase of ENOB realized automatically when signal passed through second order low pass filter :

$$V_{out}^{1}(t) = \int_{0}^{\infty} V_{in}(\xi) \bullet \exp(-\frac{(\xi - t)}{\tau}) d\xi,\ V_{out}^{2} = \int_{0}^{\infty} V_{out}^{1}(\xi) \bullet \exp(-\frac{(\xi - t)}{\tau}) d\xi$$

Improved signal presentation (left figure) facilitates numerical solution (differentiation) of the integral equation

$$V(t) = Const \bullet \int_{0}^{t} i(\xi) \exp(-\xi / \tau) d\xi$$

Solution of the equation is i(t) presented on the right figure for the cathode and two anode signals. In terms of familiar analog electronics the operation performed equivalent to differential filter on the input of spectroscopy amplifier (SA). To simulate integrating stage of the SA we implemented integration according to

$$V(t) = \int_{0}^{t} i(\xi) d\xi$$

The last operation, performed with two correlated anode waveforms, provides the pulse heights of FF.

4. Drift time determination of FF ionization

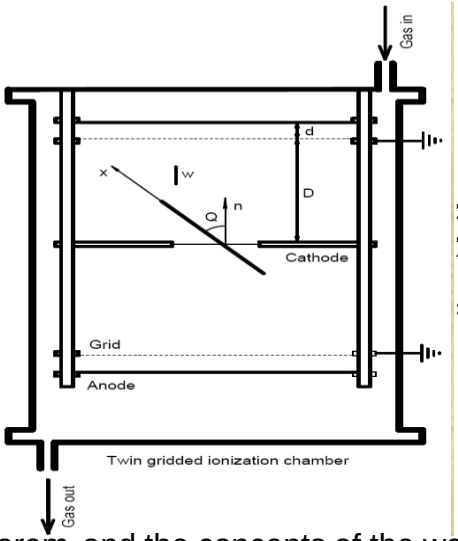

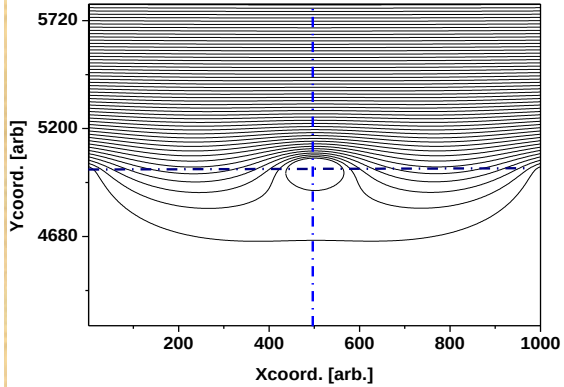

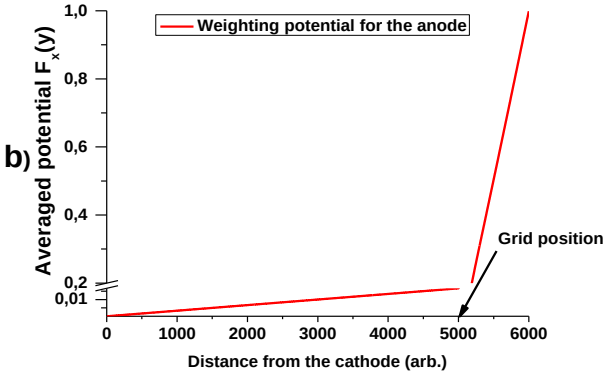

Theorem and the concepts of the weighting field and weighting potential states that the instantaneous current induced on a given electrode is equal to $i = q\bar{v}E_0$, where q is the charge of the carrier, $\bar{v}$ is its velocity, and E_0 is called the weighting field. Another way of stating the same principle is that the induced charge on the electrode is given by the product of the charge on the carrier multiplied by the difference in the weighting potential from the beginning to the end of the carrier path $Q = q\Delta\Phi$. The weighting potential as a function of position was found as the solution of the Laplace equation for the geometry of the detector with special boundary conditions. Evaluation of the ionization charge drift time can be done if the weighting potential inside the sensitive volume of the chamber is calculated as shown in the above graphs. Using explicit functions for weighting potential one can find the following expression for drift time T for ionization charge density shifting from the origin to the anode:

$$T = \frac{D}{W} \bullet \left\{ (1 - \frac{\overline{X}}{D} \bullet \cos(\Theta)) + \frac{d}{2 \bullet D} \bullet (1 - \frac{\dot{\sigma}}{1-\sigma} \bullet (1 - \frac{\overline{X}}{D} \cos(\Theta)) \right\}$$

where the meanings of d, D, Θ are clear from the sketch of the TBIC, ϭ is the grid inefficiency factor or it is the value of the average weighting potential at grid location, and X is the center for ionization charge distribution along the FF track. Parameter T for corresponding anode can be measured using the signal current waveform as follows

$$T = S / S_0, \text{ where } S = \int_0^{T_{max}} i(t) * t dt, \; S_0 = \int_0^{T_{max}} i(t) dt$$

5. FFs pulse height correction and cos(Θ) evaluation

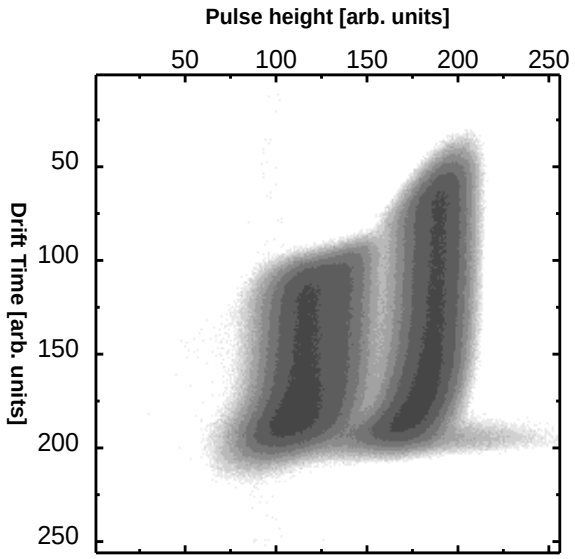

$$T = \frac{D}{W} \bullet \left\{ \left(1 - \frac{\overline{X}}{D} \bullet \cos(\Theta)\right) + \frac{d}{2 \bullet D} \bullet \left(1 - \frac{\sigma}{1-\sigma} \bullet \left(1 - \frac{\overline{X}}{D} \cos(\Theta)\right)\right)\right\}$$

$$\cos(\Theta) = \frac{T_{90} - T}{T_{90} - T_0} \qquad T_0 = T(\cos(\Theta) = 1)$$

$$T_{90} = T(\cos(\Theta) = 0)$$

$$P_A^C = P_A / \left(1 - \sigma\left(1 - \frac{T}{T_{90}}\right) \bullet \left(1 + \frac{d}{2D}\right)\right)$$

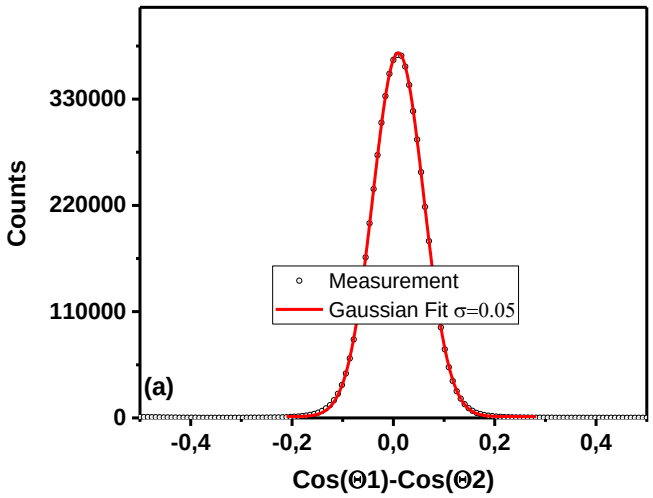

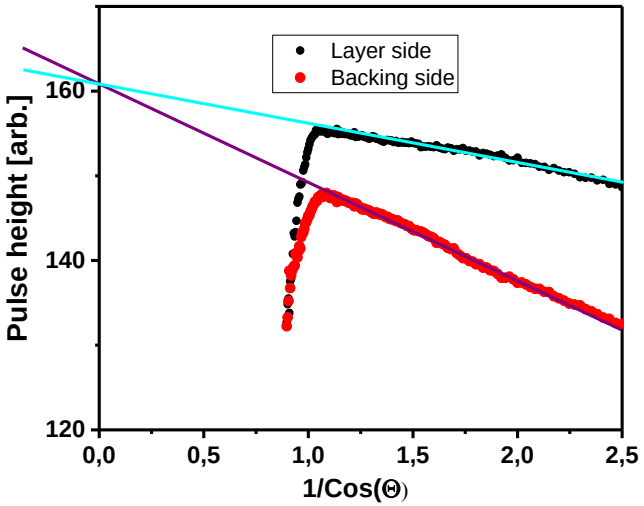

Cosine values determined according the algorithm described in previous slide are plotted in two dimensional plot of cosines measured in both halves of TBIC to demonstrate the quality of the algorithm.

6. PHD correction

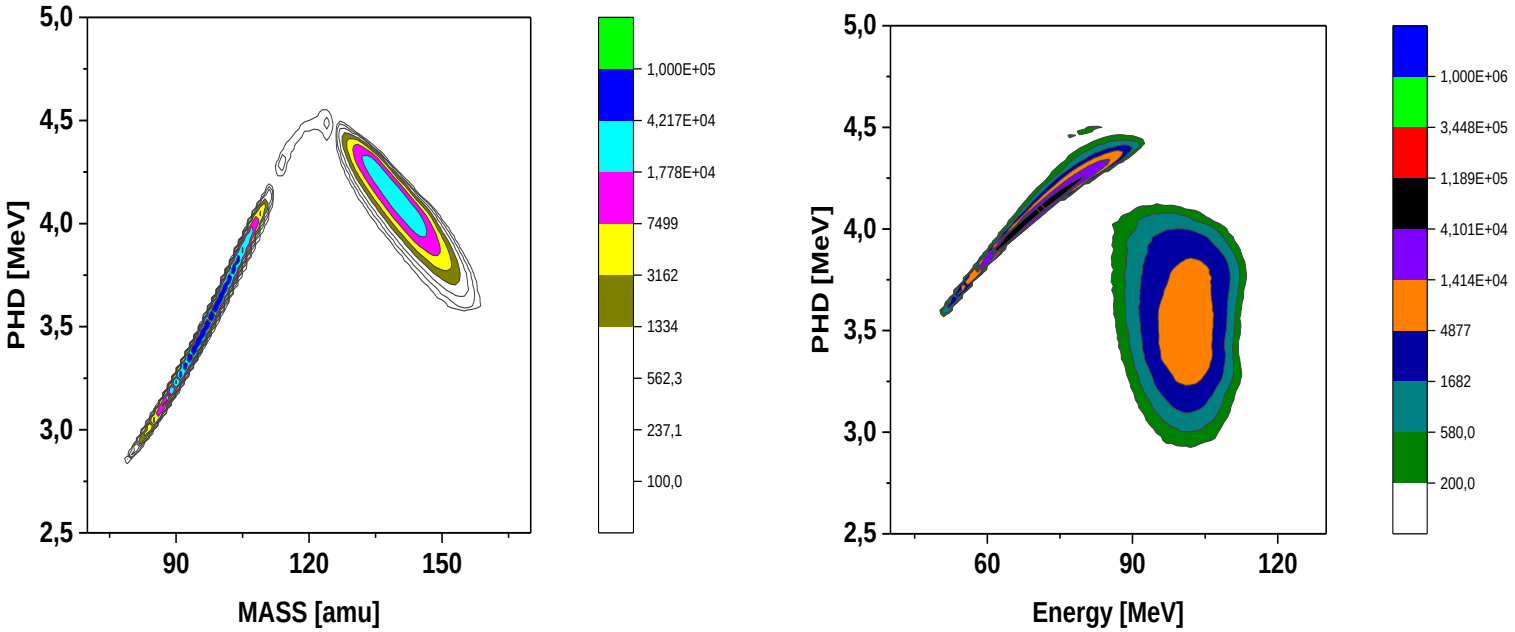

PHD was measured for P-10 working gas by C. Budtz-Jorgensen and tabulated. For FF pulse height corrections in the Ref.: F.-J. Hambsch, J. van Aarle, and R. Vogt, Nucl. Instrum. and Meth. A361, 257 (1995) the following parameteresation of the tabulated data was suggested which is more convenient for data analysis :

$$PHD(A_{post}, E_{post}) = \frac{A_{post} * E_{post}}{\alpha} + \frac{A_{post}}{\beta}$$

Parameters α, β could be fine tuned to arrive to the recent average TKE and mass values of the respective mass and THE distributions of the reaction

7. FF mass energy distribution.

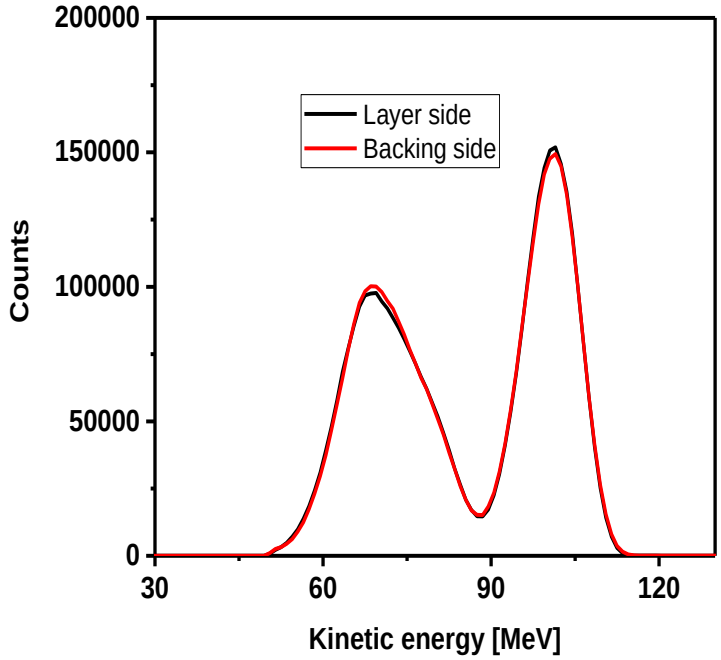

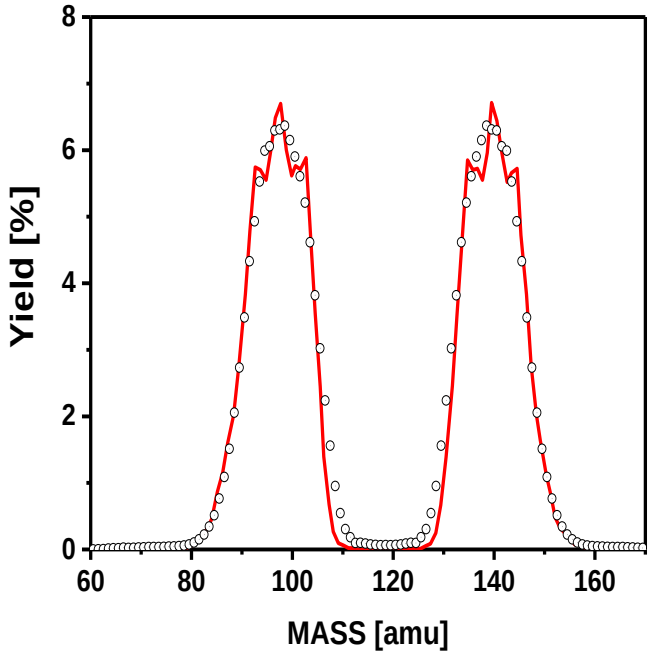

The left distribution demonstrates accuracy of implemented corrections in FFs kinetic energies. In the right plot the comparison of measured mass distribution with the literature (C. Wagemans, The Nuclear Fission Process, CRC Press, Boca Raton , FL, 1991, p. 300) is presented.

8. Constant fraction time marking for PFN TOF measurement

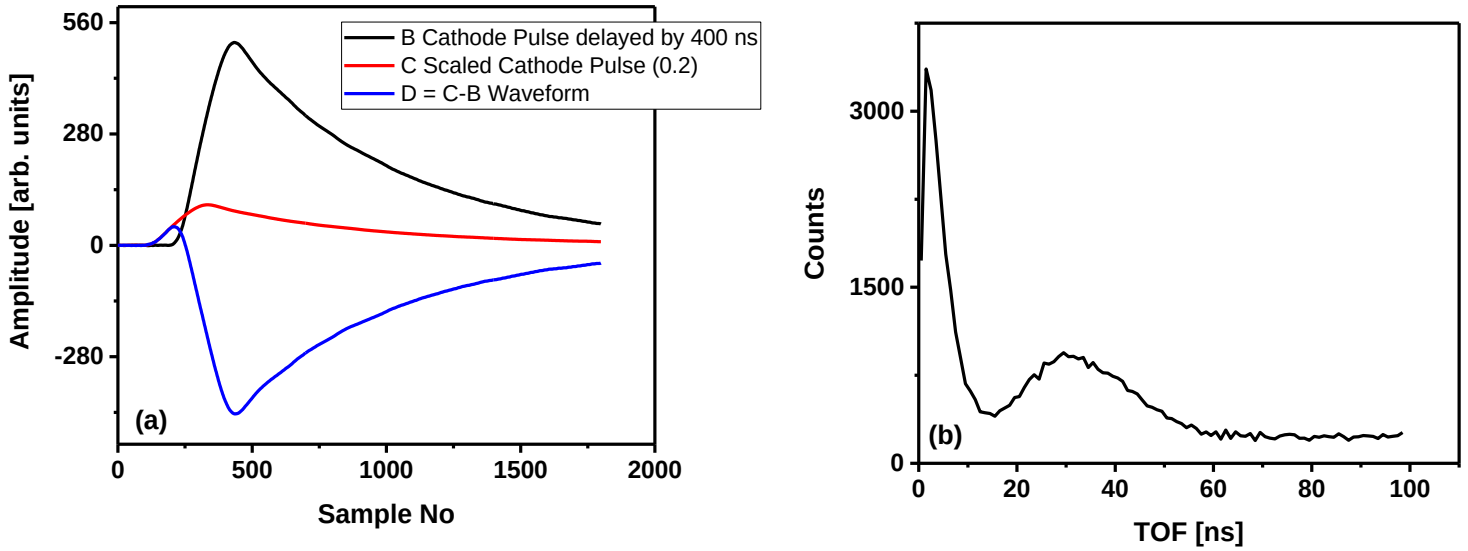

The realization of the algorithm demonstrated in Fig. (a) as it was applied to the cathode waveform.
The copy of the original signal is delayed by approximately 0.4 of the cathode signal rise time (~1000 ns) and summed with scaled (0.2) and the inverted original signal. The "T-zero" time is assigned to the crossing point of resulting signal with time axis.

9. Neutron separation from gamma radiation

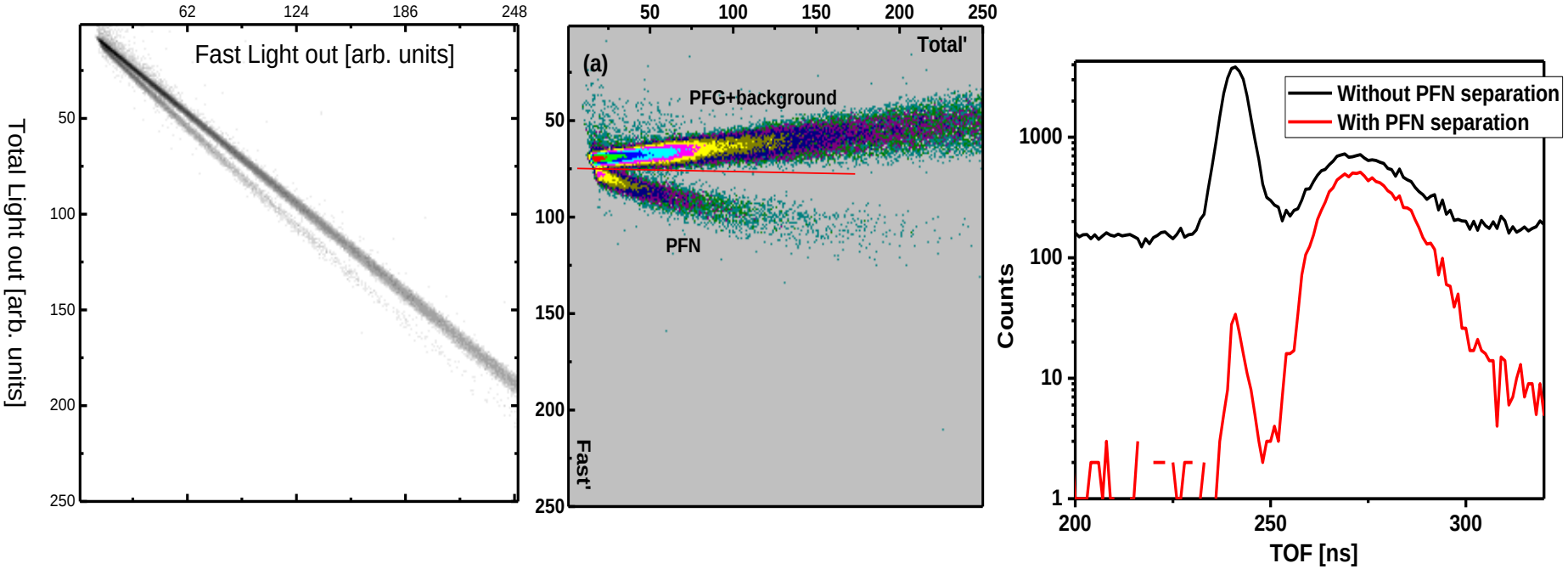

The two window algorithm (fast and total light output component) was implemented and resulted function *ND(Fast,Total)* was plotted on the upper and middle figs. demonstrates the function *ND(Fast,Total) i*n rotated according to equation

$$F' = F \bullet \cos(\Omega) + T \bullet \sin(\Omega), T' = S \bullet \{-F \bullet \sin(\Omega) + T \bullet \cos(\Omega)\}$$

,where Ω – is axes rotation angle and S>1 – is the scaling factor. Red line in the middle figure is PFN-PFG separation line . Lower figure demonstrates the TOF distribution before and after PFN separation.

10. PFN angular distribution measurement

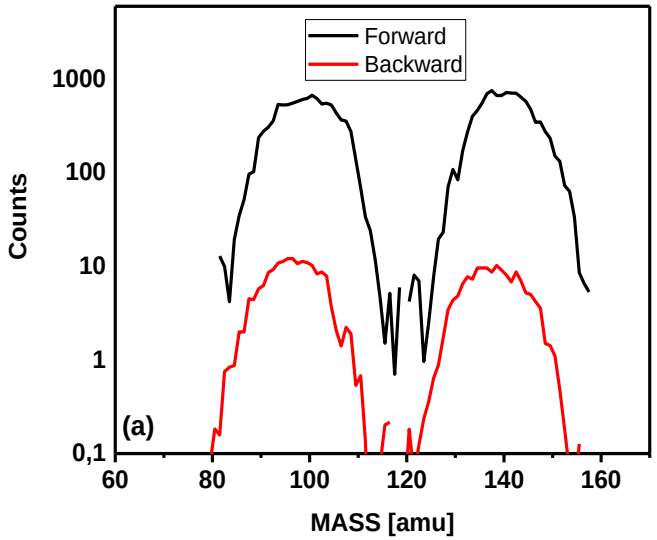

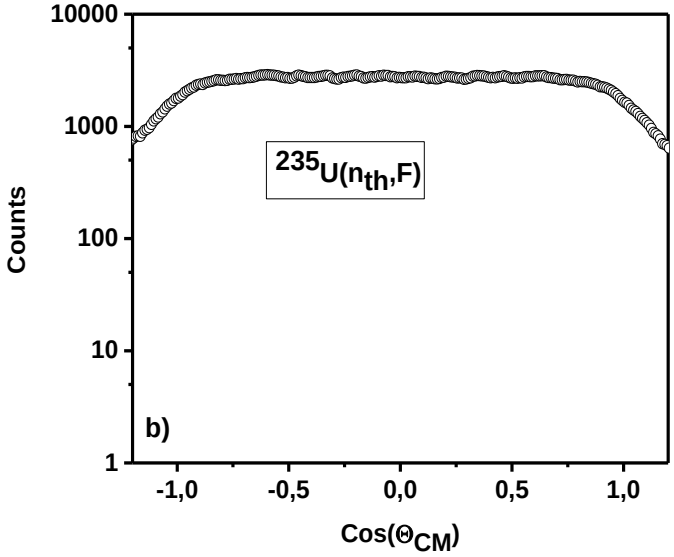

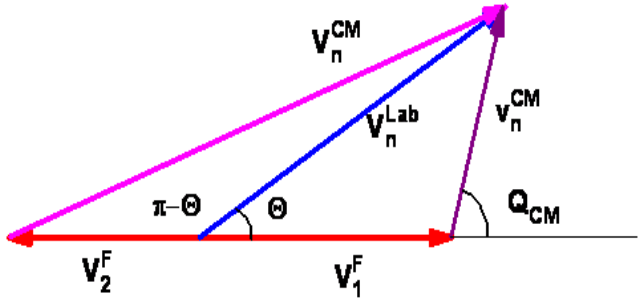

$$W_x = 1,\ W_y = \exp(E^x_{CM} - E^y_{CM})$$

C. Budtz-Jorgensen and H.-H. Knitter, Nucl. Phys., A490, 307 (1988)

11. ND efficiency evaluation

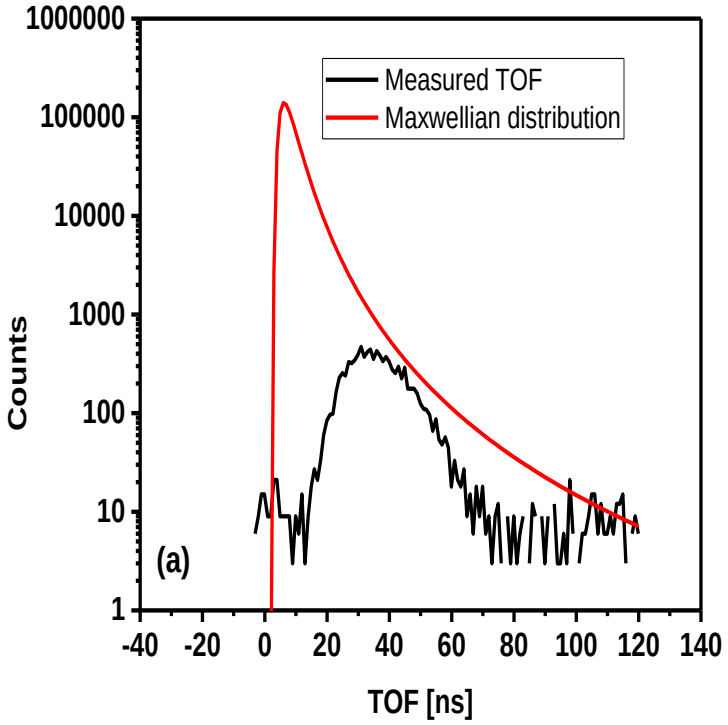

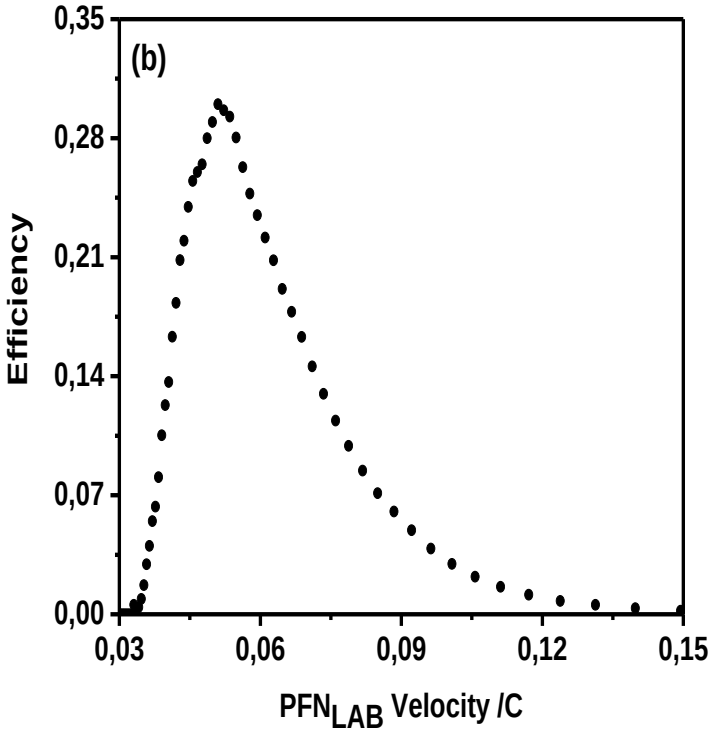

The efficiency of ND was evaluated by comparison of TOF distribution with Maxwellian distribution with the temperature parameter 1,31 MeV, $\overline{\nu} = 2.44$ and the flight path 0,65 m, Fig. (a). The conversion from TOF to PFN velocity distribution is plotted in Fig. (b).

12. PFN multiplicity on FF mass evaluation from measured data

PFN distributions evaluated in CM frame using the following transformation adopted from H.R. Bowman, J.C.D. Milton, S.G. Thompson, and W.J. Swiatecki, Phys. Rev. 129 (1963) 2133

$$\bar{\nu}(A) = \int_0^{\infty} \frac{Yc(A,TKE,V_{LAB}) \bullet V_{CM} \bullet (V_{LAB} - V_F \bullet \cos(\Theta))}{\varepsilon(V_{LAB}) \bullet V_{LAB}^2} dV_{LAB} dTKE \Big/ \int_0^{\infty} Y(A,TKE) dTKE$$

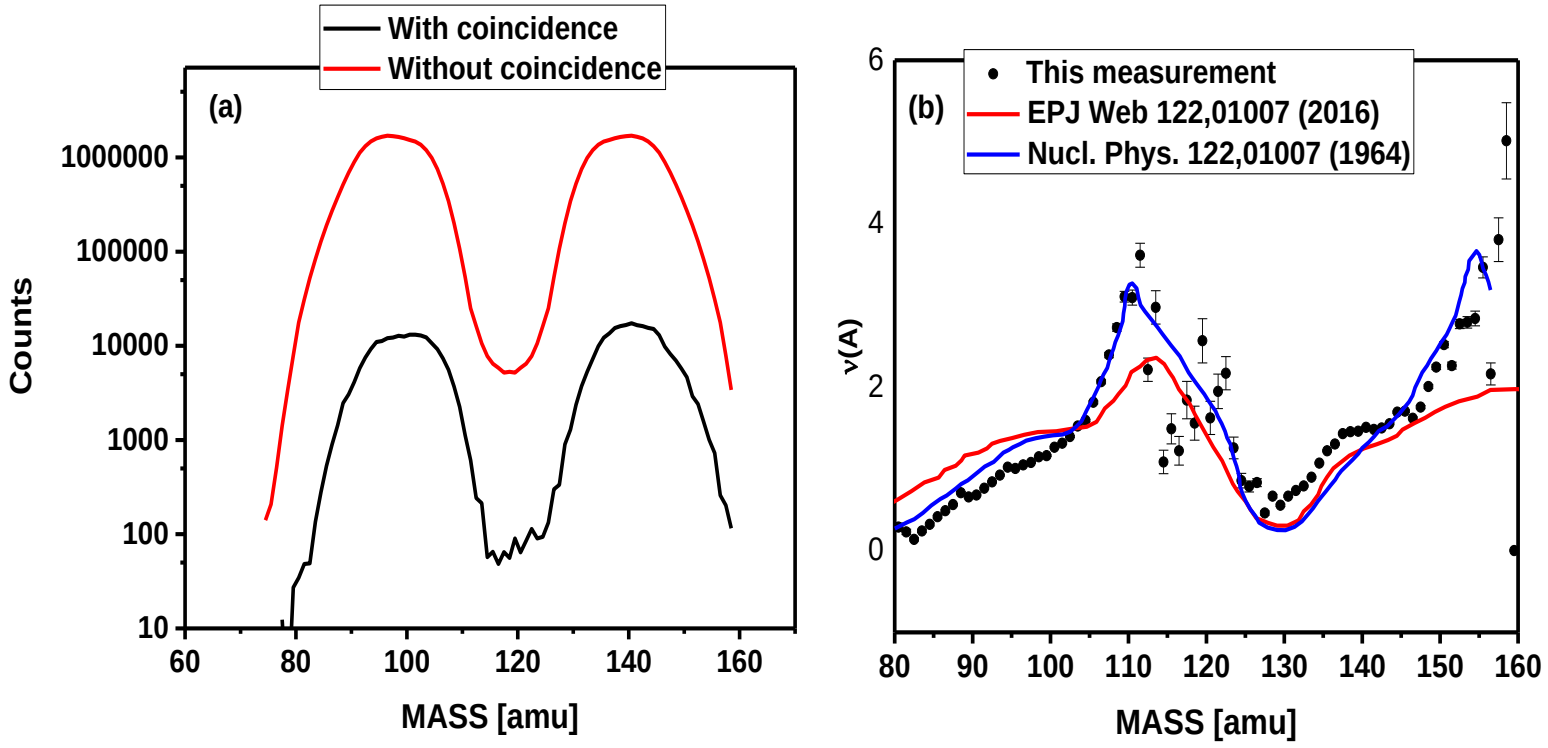

FF mass and Energy values were corrected in iterative mass&tTKE evaluation procedure, described in F.-J. Hambsch, J. van Aarle, and R. Vogt, Nucl. Instrum. and Meth. A361, 257 (1995) , but corrected for FF recoil according to A. Gavron, Nucl. Instrum. and Meth., 115 (1974) 99

13. PFN multiplicity on FF TKE evaluation from measured data

$$\bar{\nu}(TKE) = \int_0^{\infty} \frac{Yc(A, TKE, V_{LAB}) \bullet V_{CM} \bullet (V_{LAB} - V_F \bullet \cos(\Theta))}{\varepsilon(V_{LAB}) \bullet V_{LAB}^2} dV_{LAB} dA \Big/ \int_0^{\infty} Y(A, TKE) dA$$

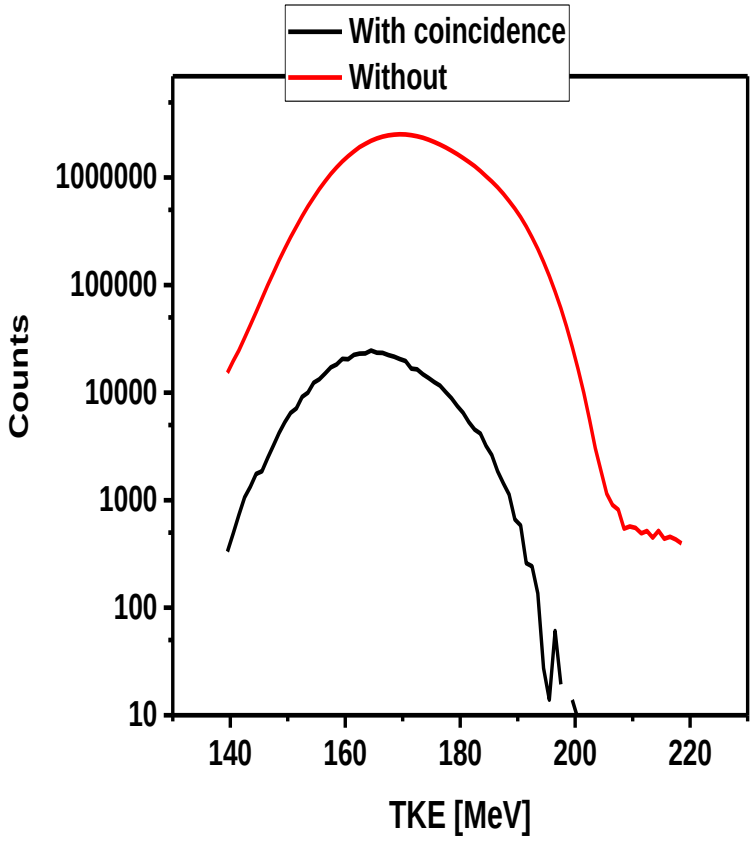

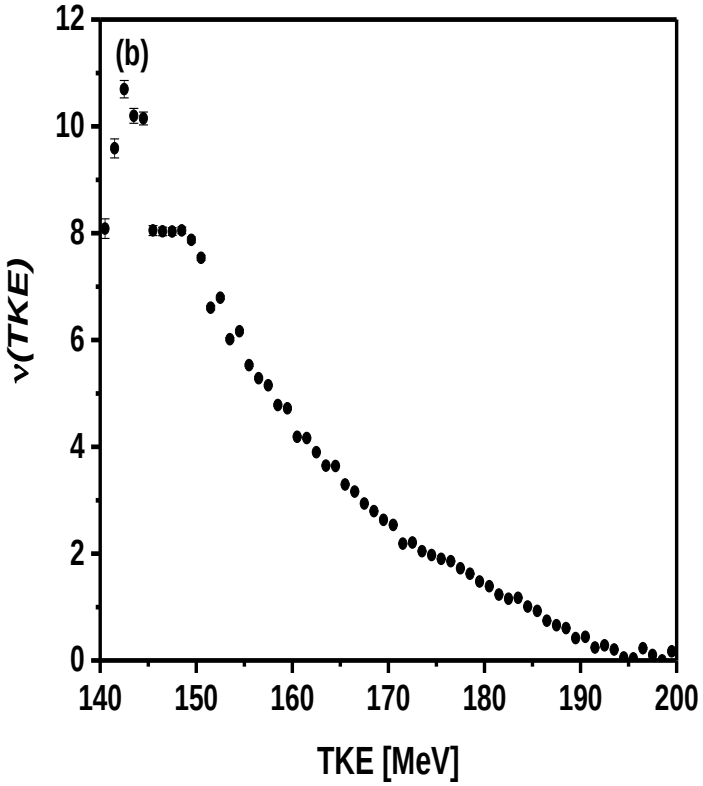

14. Conclusions

1. The digital data acquisition system was developed and tested.

2. The digital pulse processing algorithms was developed and tested both on-line and off-line.

3. The software for PFN multiplicity analysis originally developed for 252Cf(sf) experiment was revised and several bugs were removed.

4. There are some differences between result obtained in this work and the result available from the literature. This should be understood and fixed.

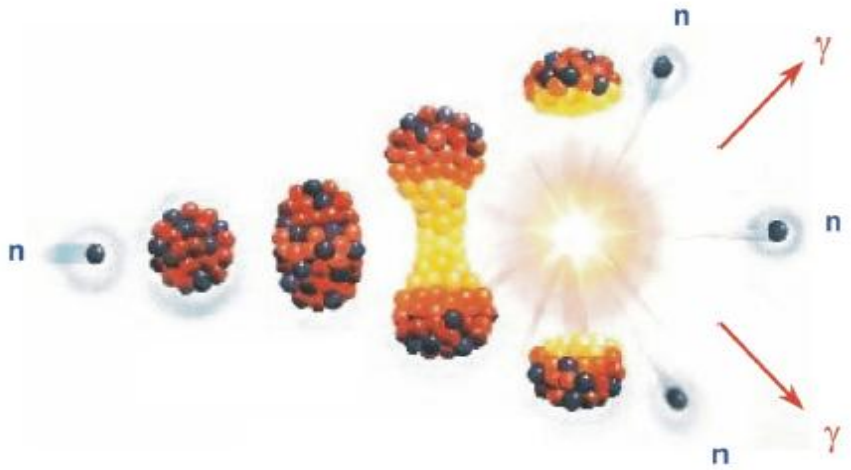

Thank you for your attention ☺